Advances in Military Technology
Vol. 21, No. 1, 2026, pp. 39-49
ISSN 1802-2308, eISSN 2533-4123
DOI 10.3849/aimt.01987

Building a Mathematical Model for Determination of the Miss Distance of Artillery Shells Using Proximity Fuzes

P. Xuan Quyen*

Faculty of System Engineering, Le Quy Don Technical University, Hanoi, Vietnam

The manuscript was received on 4 April 2025 and was accepted
after revision for publication as an original research paper on 9 February 2026.

Abstract:

This paper presents a theoretical framework for determining the miss distance of fragmentation projectiles equipped with Doppler proximity fuzes, expressed as a function of specific structural parameters. The analysis considers both the spatial offset between the antenna and the warhead detonation center (Δr) and the angular distribution of fragments, which together govern the effective lethality zone and detonation timing. The mutual influence of parameters such as the antenna–warhead separation, the projectile-target impact angle, the miss phase, and the mean fragment dispersion angle on the resulting miss distance is quantified. Numerical analysis confirms that Δr exerts the dominant influence on miss distance, while angular parameters play secondary roles. The findings highlight the critical role of Δr in realistic projectile-fuze configurations and provide a solid basis for selecting suitable structural parameters for various types of shells employing non-contact fuzes during the design process.

Keywords:

proximity fuze, radio fuze, fuze utilizing the Doppler effect, warhead

1 Introduction

Many studies have been conducted on the optimal coordination between the fragmentation flow and the antenna wavefront of proximity fuzes [1–11]. The study [1] develops a three-dimensional relative-coordinate mathematical model, formulated within a unified reference frame, to quantify the air-miss distance and burst distance of an anti-aircraft projectile employing a proximity fuze. An optical measurement methodology is applied to accurately evaluate these parameters under anti-aircraft firing conditions. The simulation study of fuzes for low-altitude surface-to-air missiles [2] discusses the anti-jamming capability and guidance of the proximity radar system.

* *Corresponding author: Faculty of System Engineering, Le Quy Don Technical University, Hoang Quoc Viet 236, Hanoi, Vietnam. Phone: +84 967 859 576, E-mail: phamxuanquyen@lqdtu.edu.vn. ORCID 0009-0000-5287-5907.*

From the perspective of target-detection theory, for non-relativistic velocities, only the longitudinal Doppler effect is dominant. Notably, at the point of closest approach between the projectile and the target, the Doppler frequency shift approaches zero, making detection at extremely short ranges particularly challenging. Therefore, detecting targets within the forward detection cone and determining its governing parameters constitute the central focus of this paper. Previous studies [8] have briefly mentioned the concept of target miss distance, yet without detailed quantitative evaluation.

Fragmentation-based munitions neutralize or damage targets through the dispersion of high-velocity fragments at a certain distance. This distance is referred to as the target miss distance of the ammunition. Analytical methods and Matlab software are employed to establish relationships between the target miss distance, detonation angle, phase of deviation, and the spatial separation between the antenna position and the detonation point. These calculations provide munition fuze designers with objective and relatively clear assessments when selecting structural parameters.

2 Methods

2.1 Coordinate System

To determine the Doppler frequency, a conical coordinate system is used in conjunction with a linear velocity coordinate system $Ox_v y_v z_v$, with its origin located at the transmitting antenna of the radar system (Fig. 1).

Axis Ox_v is parallel to the relative velocity vector $\boldsymbol{v}_{rt}$ between the ammunition and the target, coordinate plane $Ox_v y_v$ coincides with the velocity triangle plane, which is formed by the velocity vectors $\boldsymbol{v}_r ; \boldsymbol{v}_t ; \boldsymbol{v}_{rt}$. Here, $\boldsymbol{v}_r$, $\boldsymbol{v}_t$ correspond to the ammunition velocity and target velocity, respectively. The target's position at point is determined by the quantities x_v, h, ξ , where x_v represents Cartesian coordinates; h is the distance from the origin O to the projection T' of point T on plane $Oy_v z_v$, characterizing guidance accuracy and referred to as the miss distance, ξ is the polar angle, representing the phase of the miss distance. h, ξ are the polar coordinates of point T' .

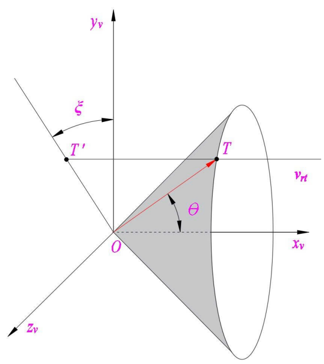

Fig. 1 Relative position of the ammunition and target in space

In Fig. 1, the relative position of the ammunition and the target in space is illustrated, with the ammunition located at O and the target positioned at T. From the coordinate system used to determine the detonation region (Figs 1 and 2), two observations can be made:

- If the miss distance $h = \text{const}$ (Fig. 1), the coordinate surface takes the form of a cylindrical shape symmetric around the Ox_v axis, representing the Doppler-undefined region.
- The $Ox_v y_v$ half-plane, which contains the positive Oy_v semi-axis and the velocity triangle (Fig. 2), corresponds to a miss distance phase value of $\xi = 0$, meanwhile, the $Ox_v y_v$ half-plane, which contains the negative Oy semi-axis (Fig. 2), corresponds to a miss distance phase value of $\xi = \pi$.

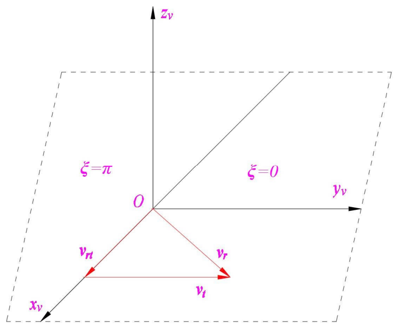

Fig. 2 The relationship between relative velocity and the phase value of the miss distance

2.2 Determination of the Target Miss Distance of the Ammunition

To describe the operation of the warhead, a coordinate system $Bx_r y_r z_r$ is typically employed, with its origin positioned at the detonation point of the warhead. The axis Bx_r aligns with the longitudinal axis of the ammunition, oriented from the center of mass toward the ammunition's nose.

When coordinating the operation of the antenna and the fragment stream, the phase of the miss distance assumes a value of $\xi \in [0, 2\pi]$. In practice, for a warhead that is symmetric along the ammunition's longitudinal axis and employs a Doppler fuze, it is possible to constrain the phase value of the miss distance $\xi = 0$ *or* $\xi = \pi$. The derivations in this section follow standard kinematic geometry, extended here to include the antenna–warhead offset Δr. These two cases are illustrated in Figs 3–4.

In Fig. 3, ε_r is the directional angle formed by the ammunition velocity vector and the relative velocity vector between the ammunition and the target; point B represents the detonation location of the warhead and is positioned from the antenna at a distance $OB = \Delta r$; α represents the average dispersion angle of the static fragments; θ is the average dispersion angle of the dynamic fragments; $\boldsymbol{v}_{\text{es}}$ denotes the velocity vector of the static fragments; $\boldsymbol{v}_{\text{ed}}$ denotes the velocity vector of the dynamic fragments; T_{es} is the intersection between the trajectory of the static fragment and a straight line containing the target, which is parallel to the x-axis; T_{ed} is the intersection between the straight line containing the target (parallel to the x-axis) and the direction of motion of the dynamic fragment; φ is the angle formed by the x-axis and the line OT_{ed}. This is the angle at which the proximity radar system decides to detonate the ammunition, commonly referred to as the detonation angle.

DOI 10.3849/aimt.01987

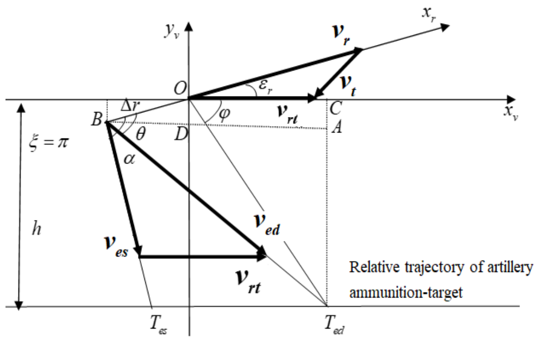

Fig. 3 Relative motion of the ammunition and target when the phase of the miss distance is $\xi = \pi$

For each miss distance h (Fig. 3), there corresponds a range of detonation angles in the velocity coordinate system, with the coordinate origin at O. The detonation command is executed when the fragment and the target meet at point T_{ed}.

Formula for calculating the velocity of dynamic fragments:

$$\boldsymbol{v}_{\text{ed}} = \boldsymbol{v}_{\text{es}} + \boldsymbol{v}_{\text{rt}} \tag{1}$$

Considering $\boldsymbol{r}_{\text{es}} = \boldsymbol{BT}_{\text{es}} = \left[r_{\text{es}x}, r_{\text{es}y}, 0 \right]$, the time required for the static fragment to travel the distance BT with speed $v_{\text{es}} \neq 0$ is:

$$t_{\text{es}} = \frac{r_{\text{es}}}{v_{\text{es}}} \tag{2}$$

Meanwhile: $r_{\text{es}} = \sqrt{r_{\text{es}x}^2 + r_{\text{es}y}^2}$. The target will be damaged if the dynamic fragment and the target meet at position T_{ed}. At that moment, the distance $T_{\text{es}}T_{\text{ed}}$ is determined by the following formula:

$$\Delta x_v = x_{vT_{\text{ed}}} - x_{vT_{\text{es}}} = t_{\text{es}} \cdot v_{\text{rt}} = \frac{r_{\text{es}} \cdot v_{\text{rt}}}{v_{\text{es}}} \tag{3}$$

Meanwhile: $x_{vT_{\text{ed}}} > x_{vT_{\text{es}}}$. Thus, the velocity vector of the dynamic fragment ($v_{\text{ed}} \neq 0$) is directed toward point T_{ed}. The time required for the dynamic fragment to travel the distance $BT_{\text{ed}} = r_{\text{ed}}$ is determined by the following formula:

$$t_{\text{ed}} = \frac{r_{\text{ed}}}{v_{\text{ed}}} \tag{4}$$

Meanwhile: $\boldsymbol{r}_{\text{ed}} = \boldsymbol{BT}_{\text{ed}} = \left[r_{\text{ed}x}, r_{\text{ed}y}, 0 \right]$.

Considering the case $\xi = \pi$, which corresponds to the situation where the target is located on the $-Oy_v$ side of the plane $Ox_v y_v$, as illustrated in Fig. 3.

In the right triangle ABT_{ed} (Fig. 3), which is right-angled at point A, we have: $\widehat{ABT_{\text{ed}}} = \theta - \varepsilon_r \neq 0$, thus $\theta \neq \varepsilon_r$.

$$AB = AT_{\text{ed}} \cdot \cot(\widehat{ABT_{\text{ed}}}) = AT_{\text{ed}} \cdot \cot(\theta - \varepsilon_r), \begin{cases} \theta \neq \varepsilon_r \\ \xi = \pi \end{cases} \tag{5}$$

In the right triangle BOD (Fig. 3), which is right-angled at point D, we have: $\widehat{OBD} = \varepsilon_r$.

$$OD = CA = OB \cdot \sin(\widehat{OBD}) = OB \cdot \sin\varepsilon_r = \Delta r \cdot \sin\varepsilon_r .$$

$$AT_{\text{ed}} = CT_{\text{ed}} - CA = h - \Delta r \cdot \sin\varepsilon_r , \; \xi = \pi \tag{6}$$

Substituting equation (6) into Eq. (5), we obtain:

$$AB = (h - \Delta r \cdot \sin\varepsilon_r) \cdot \cot(\theta - \varepsilon_r) , \begin{cases} \theta \neq \varepsilon_r \\ \xi = \pi \end{cases} \tag{7}$$

Considering the case $\xi = 0$, which corresponds to the situation where the target is located on the $+Oy_v$ side of the plane $Ox_v y_v$, as illustrated in Fig. 4.

In the right triangle ABT_{ed} (Fig. 4), which is right-angled at point A, we have: $\widehat{ABT_{\text{ed}}} = \theta + \varepsilon_r \neq 0$, thus $\theta \neq -\varepsilon_r$.

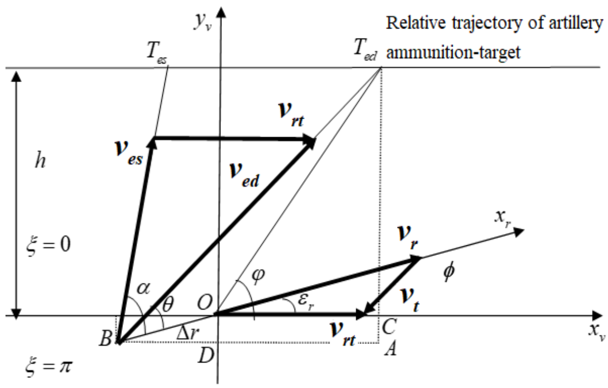

Fig. 4 Relative motion of the ammunition and target when the phase of the miss distance is $\xi = 0$

$$AB = AT_{\text{ed}} \cdot \cot\widehat{ABT_{\text{ed}}} = AT_{\text{ed}} \cdot \cot(\theta + \varepsilon_r) , \begin{cases} \xi = 0 \\ \theta \neq -\varepsilon_r \end{cases} \tag{8}$$

In the right triangle BOD (Fig. 4), which is right-angled at point D, we have: $\widehat{OBD} = \varepsilon_r$.

$$AT_{\text{ed}} = CT_{\text{ed}} + CA = h + \Delta r \cdot \sin\varepsilon_r , \; \xi = 0 \tag{9}$$

Substituting Eq. (9) into Eq. (8), we obtain:

$$AB = (h + \Delta r \cdot \sin\varepsilon_r) \cdot \cot(\theta + \varepsilon_r) , \; \xi = 0 \tag{10}$$

At this point, the analysis for $\xi = 0$ is completed. The following section focuses on determining h for both $\xi = 0$ and $\xi = \pi$ cases.

According to Figs 3 and 4, the target miss distance is determined by the following formula:

$$h = OC \cdot \cot\varphi,\ \varphi \neq 0 \tag{11}$$

$$OC = AB - BD = AB - \Delta r \cdot \cos\varepsilon_r \tag{12}$$

Substituting Eq. (7) into Eq. (12), we obtain:

$$OC = (h - \Delta r \cdot \sin\varepsilon_r) \cdot \cot(\theta - \varepsilon_r) - \Delta r \cdot \cos\varepsilon_r,\ \begin{cases} \theta \neq \varepsilon_r \\ \xi = \pi \end{cases} \tag{13}$$

Substituting Eq. (13) into Eq. (11), we obtain:

$$h = \left[(h - \Delta r \cdot \sin\varepsilon_r) \cdot \cot(\theta - \varepsilon_r) - \Delta r \cdot \cos\varepsilon_r\right] \cdot \cot\varphi_\pi,\ \begin{cases} \theta \neq \varepsilon_r \\ \xi = \pi \end{cases}$$

Thus,

$$h = \frac{\Delta r \cdot \sin\varepsilon_r \cdot \cot(\theta - \varepsilon_r) + \Delta r \cdot \cos\varepsilon_r}{\operatorname{ctg}(\theta - \varepsilon_r) - \tan\varphi_\pi},\ \begin{cases} \xi = \pi \\ \sin\varphi_\pi \neq 0 \ \Rightarrow\ \varphi_\pi \neq 0^\circ \\ \operatorname{ctg}\varphi_\pi \neq 0 \ \Rightarrow\ \varphi_\pi \neq 90^\circ \\ \sin(\theta - \varepsilon_r) \neq 0 \ \Rightarrow \theta \neq \varepsilon_r \\ \cot(\theta - \varepsilon_r) \neq \tan\varphi_\pi \end{cases} \tag{14}$$

Substituting Eq. (10) into Eq. (12), we obtain:

$$OC = (h + \Delta r \cdot \sin\varepsilon_r) \cdot \cot(\theta + \varepsilon_r) - \Delta r \cdot \cos\varepsilon_r,\ \xi = 0 \tag{15}$$

Substituting Eq. (15) into Eq. (11), we obtain:

$$h = \frac{\Delta r \cdot \sin\varepsilon_r \cdot \operatorname{ctg}(\theta - \varepsilon_r) - \Delta r \cdot \cos\varepsilon_r}{\tan\varphi_0 - \cot(\theta - \varepsilon_r)},\ \begin{cases} \xi = 0 \\ \sin\varphi_0 \neq 0 \ \Rightarrow\ \varphi_0 \neq 0^\circ \\ \operatorname{ctg}\varphi_0 \neq 0 \ \Rightarrow\ \varphi_0 \neq 90^\circ \\ \sin(\theta - \varepsilon_r) \neq 0 \ \Rightarrow \theta \neq \varepsilon_r \\ \cot(\theta - \varepsilon_r) \neq \tan\varphi_0 \end{cases} \tag{16}$$

Thus, Eqs (14) and (16) determine h corresponding to the phase shift $\xi = \pi$ and $\xi = 0$.

3 Results and Discussion

The assessment of the target miss distance of the ammunition depends on several parameters, such as the detonation angle, the distance between the antenna and detonation point, the directional angle, the fragmentation dispersion angle and the phase of the miss distance. This dependence can be analyzed through several representative configurations.

In the first configuration, $\theta = 30°$; $\varepsilon_r = 15°$; $\varphi \in [0°, 60°]$; $\Delta r = 0.3\,\text{m}$; $\xi = \pi$ or $\xi = 0$. The purpose of applying formulas (14) and (16) is to determine the target miss distance of the ammunition. The values are calculated using Matlab software (Fig. 5).

From Figs 3–5, as well as Eqs (14) and (16), it can be observed that at position *B* (Figs 3 and 4), the detonation angle φ reaches its maximum value. When *h* gradually increases from $\Delta r \sin\varepsilon_r$, the value of φ gradually decreases and fluctuates slightly around the asymptotic value corresponding to the miss distance, ranging from 5 m to 20 m.

In Fig. 5, *PhiPiAS5-20* and *Phi0AS5-20* denote the computational procedures developed by the authors to determine the arithmetic mean detonation angles of the projectile, calculated over the miss-distance interval from 5 m to 20 m using MATLAB's built-in mean() function, which performs an arithmetic average of the computed values. According to the computational analysis presented in Fig. 5, the mean detonation angle is $PhiPiAS5\text{-}20 = 14.95°$ for the miss-distance range of 5 m to 20 m at a phase value of $\xi = \pi$, and $Phi0AS5\text{-}20 = 38.64°$ for the same range at $\xi = 0$. The detonation angle φ is allowed to fluctuate within the ranges $[14.95°, 27.86°]$ for $\xi = \pi$ and $[38.64°, 58.29°]$ for $\xi = 0$, when the miss distance is less than 5 m.

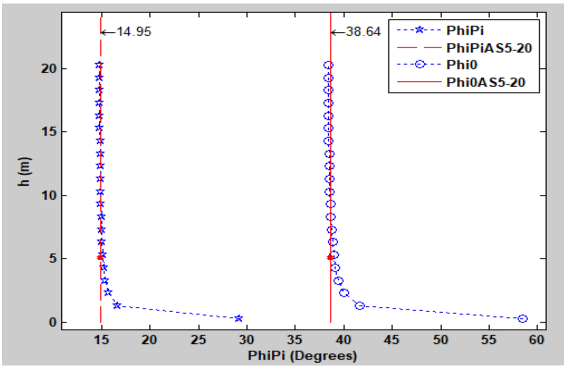

Fig. 5 The target miss distance of the ammunition depending on the detonation angle for the phase of the miss distance $\xi = \pi$ and $\xi = 0$

In a subsequent study, to comprehensively evaluate the parametric dependence of the miss distance *h* on the geometric and kinematic factors in Eqs (14) and (16), a series of numerical simulations were performed by varying φ, θ, ε_r, Δr within representative operational ranges. The obtained results are presented in Figs 6–8, where each figure isolates the influence of a specific parameter pair while keeping others constant to facilitate clear interpretation.

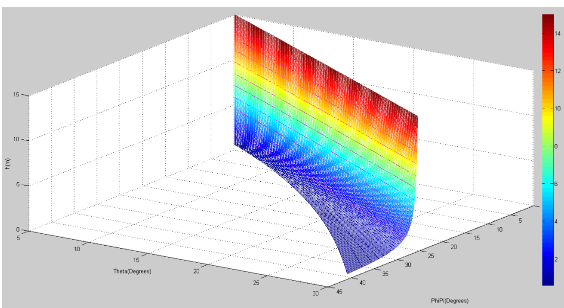

Fig. 6 The miss distance h as a function of φ and θ

DOI 10.3849/aimt.01987

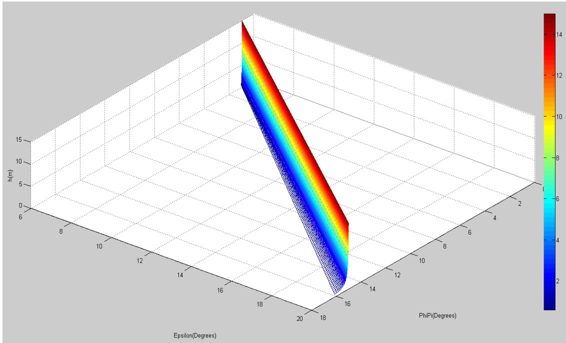

Fig. 7 The miss distance h as a function φ *of* ε_r *and*

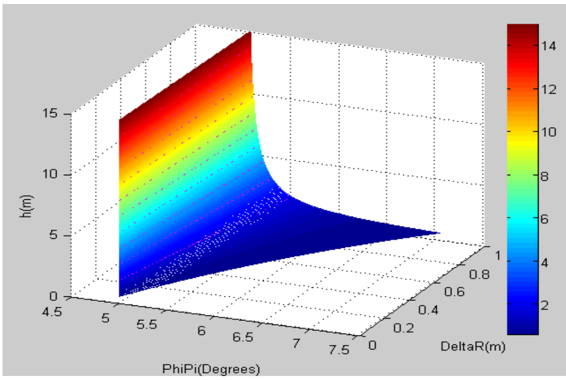

Fig. 8 The miss distance h as a function of φ *and* Δr

The combined numerical evidence of Figs 6–8, supported, indicates that the miss distance h is principally controlled by the antenna-warhead offset Δr (linear scaling). The heading angle ε_r constitutes the next most significant parameter, producing an approximately linear modulation of h within the examined interval. The fragmentation dispersion angle θ exerts a secondary, coupled effect through $\theta - \varepsilon_r$. The detonation angle φ has only a minor effect on h for typical operating points; however, φ can induce extreme sensitivity when the denominator $\cot(\theta - \varepsilon_r) - \tan\varphi \to 0$. Hence, practical design guidance is twofold: Minimize Δr where feasible and avoid operational configurations that render the denominator small.

These findings are corroborated by gradient analyses and numerical sweeps; additional robustness tests (grid refinement and Monte–Carlo perturbations) have been performed to confirm stability within the studied parameter domain (Figs 9–12).

The computational analysis presented in Figs 9–12 investigates how the miss distance h varies as a function of key structural and kinematic parameters, including ε_r and φ. The obtained 3D surface maps demonstrate (Fig. 9) that h exhibits a strong and nearly linear dependence on ε_r in the examined range (6°–20°), whereas its sensitivity to the detonation angle remains minor. This indicates that Δr governs the effective miss distance of the projectile.

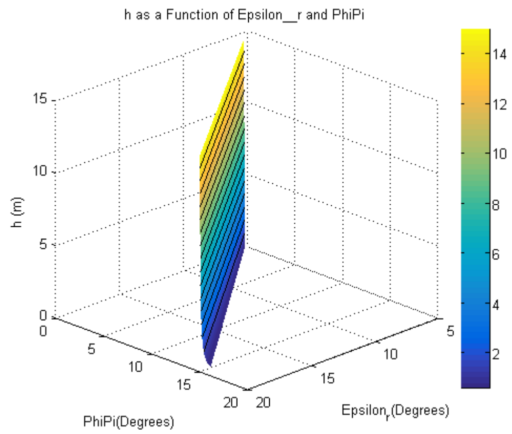

Fig. 9 The miss distance h as a function of φ *and* ε_r

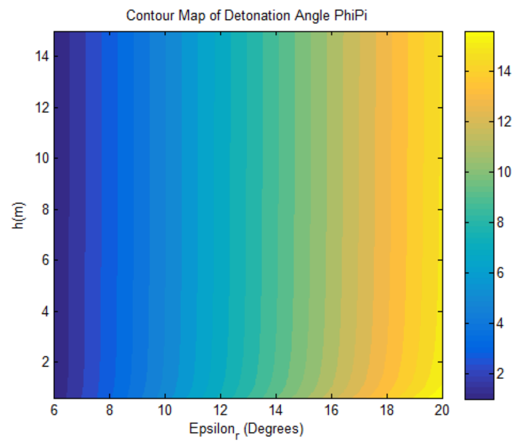

Fig. 10 Contour map of detonation angle φ

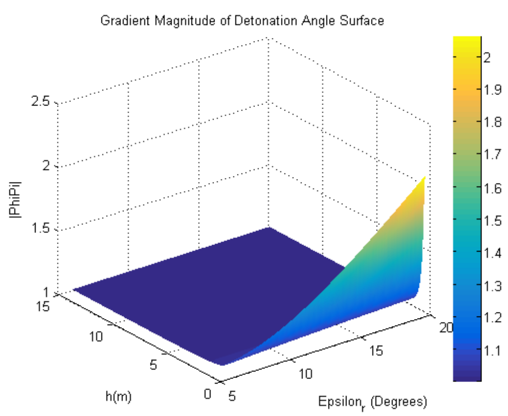

Fig. 11 Gradient magnitude of φ *surface*

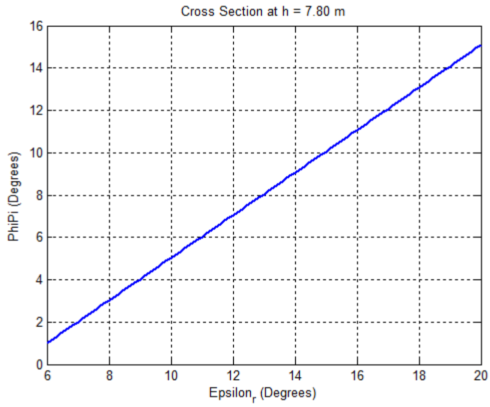

Fig. 12 Cross section at h = 7.80m

The computational analysis presented in Figs 9–12 investigates how the miss distance h varies as a function of key structural and kinematic parameters, including ε_r and φ. The obtained 3D surface maps demonstrate (Fig. 9) that h exhibits a strong and nearly linear dependence on ε_r in the examined range (6°–20°), whereas its sensitivity to the detonation angle remains minor. This indicates that Δr governs the effective miss distance of the projectile.

The gradient magnitude (Fig. 11) analysis further supports this observation, revealing that the local variations of h with respect to ε_r are modest and well-behaved throughout the studied domain. This stability suggests that moderate deviations in the engagement geometry will not significantly affect the proximity fuze's detonation timing or the resulting fragmentation pattern.

The contour and cross-sectional plots (Figs 10, 12) provide a clear visual interpretation of these dependencies. As ε_r increases, h follows a monotonic trend, confirming the analytical expressions derived in Section 2. In contrast, the influence of altitude-related factors and small geometric perturbations on h remains secondary.

To ensure generality, the simulations were extended across a continuous range of $\Delta r, \varepsilon_r, \varphi, \theta$ values (as shown in Figs 6–12), allowing the functional behavior of $h(\Delta r, \varepsilon_r, \varphi, \theta)$ to be quantitatively characterized. The numerical analysis in this study was conducted for a miss distance range up to 15 m, which corresponds to the effective fragment dispersion zone. However, the proposed mathematical model remains valid for larger distances as well.

Overall, these results establish that the miss distance h can be effectively predicted and optimized through precise control of the antenna–detonation separation Δr and the directional angle ε_r. This analytical-numerical framework provides a valuable foundation for improving Doppler-based proximity fuze design and enhancing hit probability in anti-aircraft ammunition systems.

4 Conclusion

Solving Eqs (14) and (16) enables the determination of the ammunition's miss distance for specific structural parameters. The interpretations and analyses above provide a foundation for identifying additional parameters of the proximity fuze, such as ammunition-target contact angle φ, miss phase ξ, distance between the antenna and detonation point Δr , average fragment dispersion angle θ, which is crucial for proximity fuze design. The ongoing research by the authors focuses on refining the parameter set and developing enhanced numerical solution methods to extend the applicability of the proposed framework. The outcomes of this work will be reported in a subsequent publication. The present findings also open potential directions for future developments, such as multi-point detonation control, compact antenna configurations for universal fuze integration, and quantitative assessment of target survivability after fragmentation impact.

References

[1] HUO, H., C. DONG, J. LI and Y. WANG. Measurement Method of the Air-Miss Distance and Explosion Distance of Proximity Fuze. In*: 2018 International Conference on Chinese Automation Congress (CAC).* Xi'an: IEEE, 2018, pp. 3924-3929. DOI 10.1109/CAC.2018.8623450.

[2] ZHAO, Q., et al. Simulation Design of Fuze-Warhead System of Air-Defense Missile at Very Low Altitude. *Journal of Systems Engineering and Electronics*, 2017, **28**(3), pp. 572-584. DOI 10.21629/JSEE.2017.03.17.

[3] ARORA, V.K. *Proximity Fuzes: Theory and Techniques*. New Delhi: Defence Research & Development Organisation, 2010. ISBN 978-81-86514-29-0.

[4] KOLODNY, M.A. Radar Proximity Fuzing and the Cold War Paradigm. In*: 2011 IEEE MTT-S International Microwave Symposium (MTT-S).* Baltimore: IEEE, 2011. DOI 10.1109/MWSYM.2011.5973333.

[5] LI, Z.B. Implementation and Development of Compact UWB Proximity Fuze Sensor System. In*: 2011 International Conference on Computational Problem-Solving (ICCP).* Chengdu: IEEE, 2011, pp. 120-122. DOI 10.1109/ICCPS. 2011.6092218.

[6] NASSER, A., F. AHMED, K.H. MOUSTAFA and A. ELSHABRAWY. Recent Advancements in Proximity Fuzes Technology. *International Journal of Engineering Research and Technology*, 2015, **4**(4), pp. 1233-1238. DOI 10.17577/ IJERTV4IS041400.

[7] ZHANG, X. and H. LI. Calculation Model of Projectile Explosion Position by Using Acousto-Optic Combination Mechanism. *IEEE Access*, 2021, **9**, pp. 126058-126064. DOI 10.1109/ACCESS.2021.3109918.

[8] QUYEN, P.X. Determining the Dependence of Doppler Frequency on the Slip Between the Artillery Shell and the Target When Using a Doppler Non-Contact Fuze. *Journal of Natural Science – Engineering and Technology* (in Vietnamese), 2023, **228**(02). DOI 10.34238/tnu-jst.7226.

[9] SHI, X., Y. YUAN, S. CHEN, S. ZHANG and H. ZHAO. The Research on Damage Effect of Target under the Action of Fragmentation Warhead. In*: 2021 IEEE 6th International Conference on Signal and Image Processing (ICSIP).* Nanjing: IEEE, 2021, pp. 1150-1154. DOI 10.1109/ICSIP52628.2021.9688776.

[10] LI, H., X. ZHANG, X. ZHANG and J. GAO. Warhead Fragments' Distribution Measurement Method by a Multiscreen Sensors' Intersection Test Mechanism and Equivalent Target Damage Probability Calculation. *IEEE Transactions on Instrumentation and Measurement*, 2021, **70**, 7004109. DOI 10.1109/TIM.2021.3079557.

[11] ZHANG, X. and H. LI. A Target Damage Assessment Mathematical Model and Calculation Method Based on the Intersection of Warhead Fragment and Target Mechanism. *Mathematics*, 2022, **10**(17), 3101. DOI 10.3390/math10173101.